# Forward modelling with application to A-Train observations

**Alejandro Bodas-Salcedo**

*Met Office Hadley Centre, Exeter*
*EX1 3PB, United Kingdom*
*alejandro.bodas@metoffice.gov.uk*

**ABSTRACT**

Clouds and their radiative properties are still not sufficiently well represented in numerical weather prediction (NWP) and climate models. Improving their representation is a key priority, as clouds play a main role in the Earth's radiation budget and are a key uncertainty in predictions of climate change. In this paper I discuss the utility of forward modelling as a tool to better exploit the current suite of satellite observations for the evaluation of clouds in models. An overview of model evaluation using satellite retrievals and some initial applications of the use of forward modelling in model evaluation is presented. I also focus on recent aplications to the active instruments on the A-Train, and I introduce a new tool that should help to exploit the new observing capabilities brought by the A-Train.

## 1 Introduction

General circulation models (GCMs) of the atmosphere, like those used for numerical weather prediction (NWP) and climate projections, operate with resolutions from a few kilometres to hundreds of kilometres. Many atmospheric processes, like turbulence and microphysical processes within clouds, operate at smaller scales and hence cannot be resolved by the current model resolutions. These processes are included by means of parameterisations, which are semi-empirical or statistical models that relate gridbox mean variables to these subgrid processes. For instance, some cloud parameterisations diagnose the amount of cloud condensate in the fraction of the gridbox that it occupies (cloud area fraction) with the relative humidity of the gridbox (Slingo, 1982; Smith, 1990). The formulation of these parameterisations are very important in the model evolution as they directly modify the three-dimensional structure of temperature and humidity (e.g. condensation/evaporation) or indirectly by interacting with other parameterisations (e.g. radiation). Therefore, the evaluation of these parameterisations is crucial to improve our weather forecasts or increase our confidence in climate projections.

Satellites have proven to be very helpful tools for this purpose as they provide global or nearly-global coverage, therefore giving a representative sample of all meteorological conditions. However, satellites do not measure directly those geophysical quantities of interest, like the amount or phase of the cloud condensate. They measure the intensity of radiation coming from a particular area in a particular wavelength range (radiances). The range of wavelengths covered by past and current systems span several orders of magnitude, from the ultra-violet ($10^{-7}$ m) to radio frequencies (1 m). Then, information on the geophysical quantities of interest is inferred by inverse modelling, usually called satellite retrievals (Stephens and Kummerow, 2007). Satellite retrievals have been used in numerous studies to analyse the performance of NWP and climate models (e.g. Gates et al., 1999; Allan et al., 2007; Bodas-Salcedo et al., 2008a).

There are two main physical processes by which radiation interacts with matter: absorption and scattering. During absorption processes, the incident radiation is converted into a different form of energy. In scattering processes, the incident radiation is dispersed in a different direction. The total amount of

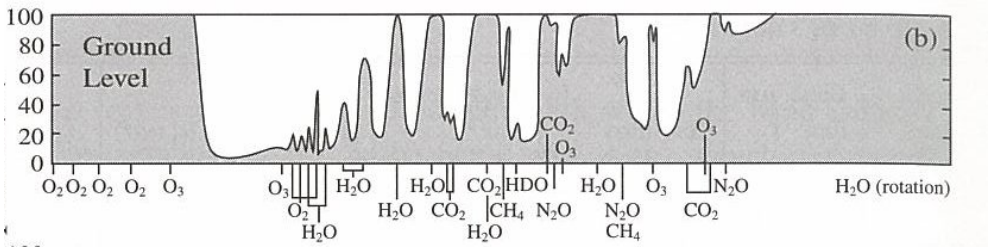


*Figure 1: Absorption spectrum (in %) for the entire vertical extent of the atmosphere (from Thomas and Stamnes, 2002).*

energy from the original direction of the incident beam is measured by the extinction coefficient. The different constituents of the atmosphere absorb radiation in many different wavelenghts, producing a total absorption spectrum with regions that are completely opaque and others that are partially or almost completely transparent to radiation (Figure 1). The efficiency by which energy of a radiation beam is removed from the incident direction is measured by the scattering efficiency ($Q_s$), and depends on the ratio between the size of the particle and the wavelength of the incident radiation, measured by the size parameter $\xi = 2\pi r/\lambda$, where $r$ is the radius of the particle and $\lambda$ the wavelength of the incident radiation (Table 1). The type of scattering is divided in three main regimes, depending on the magnitude of the size parameter: Rayleigh regime for $\xi \ll 1$, Mie regime for $\xi$ of the order of 1, and $\xi \gg 1$. There are many text books that cover the topic of atmospheric radiation in great detail (e.g. Liou, 2002; Thomas and Stamnes, 2002). Remote sensing systems make use of these radiative properties to infer physical properties about the atmospheric constituents. Stephens and Kummerow (2007) review most of the techniques used in satellite retrievals of clouds and precipitation.

| | | Size parameter | | |
|---|---|---|---|---|
| | Size (a) | λ=0.5 μm | λ=10 μm | λ=1 cm |
| Aerosol | 1 μm | $1.26 \times 10^{1}$ | $6.3 \times 10^{-1}$ | $6.3 \times 10^{-4}$ |
| Water droplet | 10 μm | $1.26 \times 10^{2}$ | $6.3 \times 10^{0}$ | $6.3 \times 10^{-3}$ |
| Ice crystal | 100 μm | $1.26 \times 10^{3}$ | $6.3 \times 10^{1}$ | $6.3 \times 10^{-2}$ |
| Raindrop | 1 mm | $1.26 \times 10^{4}$ | $6.3 \times 10^{2}$ | $6.3 \times 10^{-1}$ |
| Snowflake | 1 cm | $1.26 \times 10^{5}$ | $6.3 \times 10^{3}$ | $6.3 \times 10^{0}$ |
| | | Rayleigh | Mie | G. Optics |

*Table 1: Size parameter ($\xi = 2\pi r/\lambda$ for typical sizes of different atmospheric particles and typical wavelengths) (adapted from Liou, 2002). The shading denotes (aproximately) the regime for each combination of size and wavelength.*

Forward modelling is at the core of satellite retrievals (Stephens and Kummerow, 2007), although it can be used as an independent tool. I will focus on the use of forward modelling as a tool to evaluate models. The main motivation of model evaluation is to highlight model errors and help to improve the parameterizations. By improving the model parameterizations we hope to improve weather forecasts and the reliability of climate projections. The remainder of this paper is organised as follows: section 2 presents and overview of model evaluation using satellite retrievals; section 3 shows some initial applications of the use of forward modelling in model evaluation; section 4 extends this to recent applications using the A-Train, and conclusions are presented in section 6.

## 2 Model evaluation using satellite retrievals: a brief overview

Satellite data have been used to evaluate NWP and climate models since the early days of Earth observation. Slingo (1982) used observations from satellites to obtain a global perspective of the energetics of the current Met Office model at the time. This study first assessed the quality of the simulation of the seasonal cycle of TOA fluxes by comparing model outputs with the satellite-derived radiative fluxes. The simulations compared favourably with the observations, so the model was used to understand some aspects of the seasonal cycle of TOA radiation budget. Since then, Earth radiation budget measurements, both at the top of the atmosphere and the surface, have been routinely used in model evaluation, and there are many examples in the literature (e.g. Bodas-Salcedo et al., 2008a, and references therein).

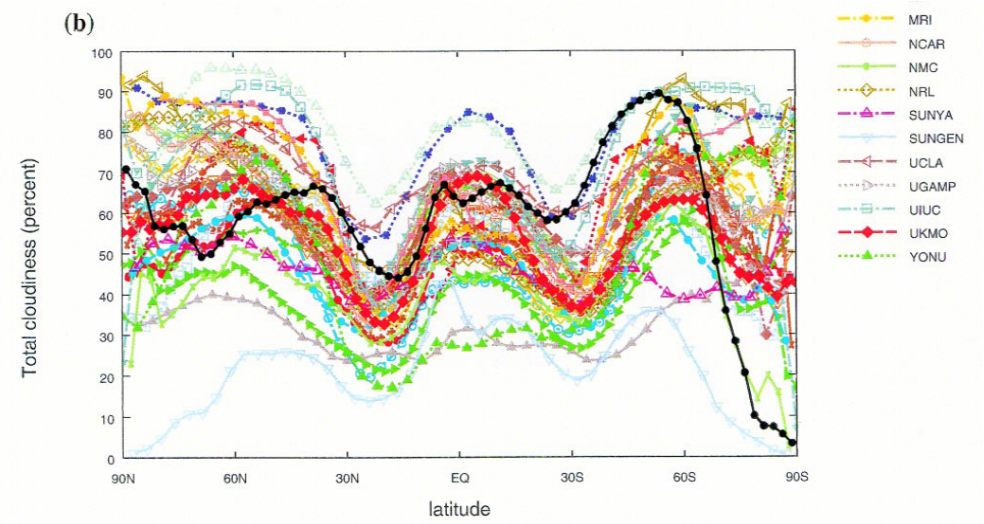


*Figure 2: (from Gates and 15 coauthors, 1999).*

There are many examples of the use of satellite retrievals in model evaluation. Gates and 15 coauthors (1999) show the results of the Atmospehric Model Intercomparison Project (AMIP), that undertook the systematic validation, diagnosis, and intercomparison of the performance of atmospheric general circulation models. Figure 2 shows a comparison of the zonal mean DJF cloud cover as simulated by the 35 participant models versus the retrievals from the International Satellite Cloud Climatology Project (ISCCP, Rossow and Schiffer, 1999). The differences between models and with respect to the observations are large. Differences still remain large in similar comparisons with current generations of models. However, it is very difficult ot extract quantitative information from these type of comparisons. Part of the scatter in the models' results stems from the different definitions of total cloudiness among models and between the models and ISCCP. On top of that, satellite sensors have limitations: finite sensitivity, fixed viewing geometry, etc, that introduce uncertainties on the retrievals. Figure 3 shows the uncertainty associated with retrievals of cloud cover from different satellite instruments and using different retrieval techniques. Another source of error is the a priori information used in the retrievals. Eyre (1987) showed that biases in the a priori information (or first guess) used in linear retrievals can introduce biases in the climatological estimates of atmospheric properties.

## 3 Model evaluation using forward modelling: initial applications

In the last two decades, a different avenue has been followed to exploit satellite data in model evaluation: the use of forward modelling of basic satellite measurements from model fields. Morcrette (1991) simulated radiances in the LW window channel of METEOSAT from ECMWF model fields using the

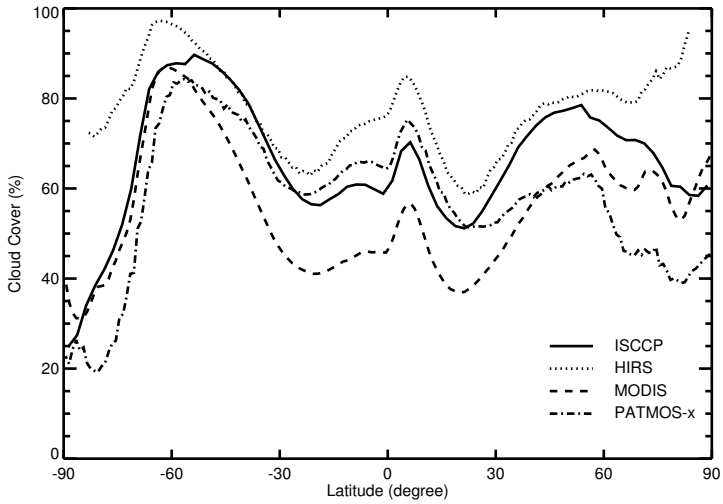


*Figure 3: Zonal mean cloud cover from several satellite cloud retrievals: ISCCP-D2, HIRS, MODIS, and PATMOS-X. Figure courtesy of Jonny Williams.*

correct satellite geometry, and converted them to brightness temperatures using the METEOSAT filter function. By plotting frequency histograms of $T_b$ as function of time (evolution histograms) he was able to study the diurnal cycle of surface temperature and cloudiness in several selected regions. Figure 4 one shows one example for an area covering Nigeria. It shows the development of the convection in 6 to 9h, whereas the dissipation takes place in 12 to 15 h. The model diurnal cycle of surface temperature is smaller than in the observations. He concluded that the underestimated amplitude of the diurnal cycle of the surface temperature might come from too small a resistance for evapotranspiration from the vegetation or alternatively a cloud cover that is too efficient at decreasing the downward solar radiation.

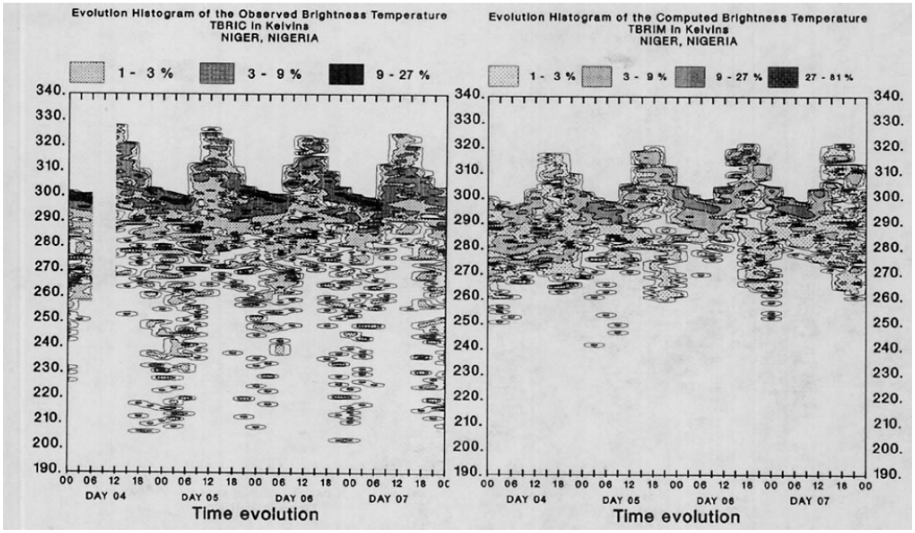


*Figure 4: Evolution histogram of the window brightness temperature $EH(T_b)$ over Nigeria. Left: constructed from ISCCP data averaged over the 81 $(1.125)^2$ model gridboxes present in the limited area. Right: constructed from the simulated brightness temperatures from the 81 model gridboxes (from Morcrette, 1991).*

A similar approach was followed by Soden and Bretherton (1994). They simulated clear-sky $T_b$ in the 6.7 $\mu m$ channel of GOES from the ECMWF and NCAR CCM models and compare these fields with

the observations. The $T_{6.7}$ is primarily sensitive to relative humidity vertically averaged over a range of pressures in the upper troposphere extending from roughly 200 to 500 hPa. Warm temperatures indicate a dry upper troppposphere whereas cold temperatures correspond to wet troposphere. Figure 5 shows the comparison for July 1987. It shows large discrepancies related to the influence of large-scale dynamical processes in determining the distribution of upper tropospheric humidity (UTH). In particular, the ECMWF model exhibits a distinct dry bias along the Intertropical Convergence Zone (ITCZ) and a moist bias over the subtropical descending branches of the Hadley cell, suggesting an underprediction in the strength of the Hadley circulation. The CCM, on the other hand, demonstrates greater discrepancies in UTH than are observed for the ECMWF model, but none that are as clearly correlated with well-known features of the large-scale circulation. Other authors have also used this approach in model evaluation (e.g. Salathé and Chesters, 1995; Ringer et al., 2003).

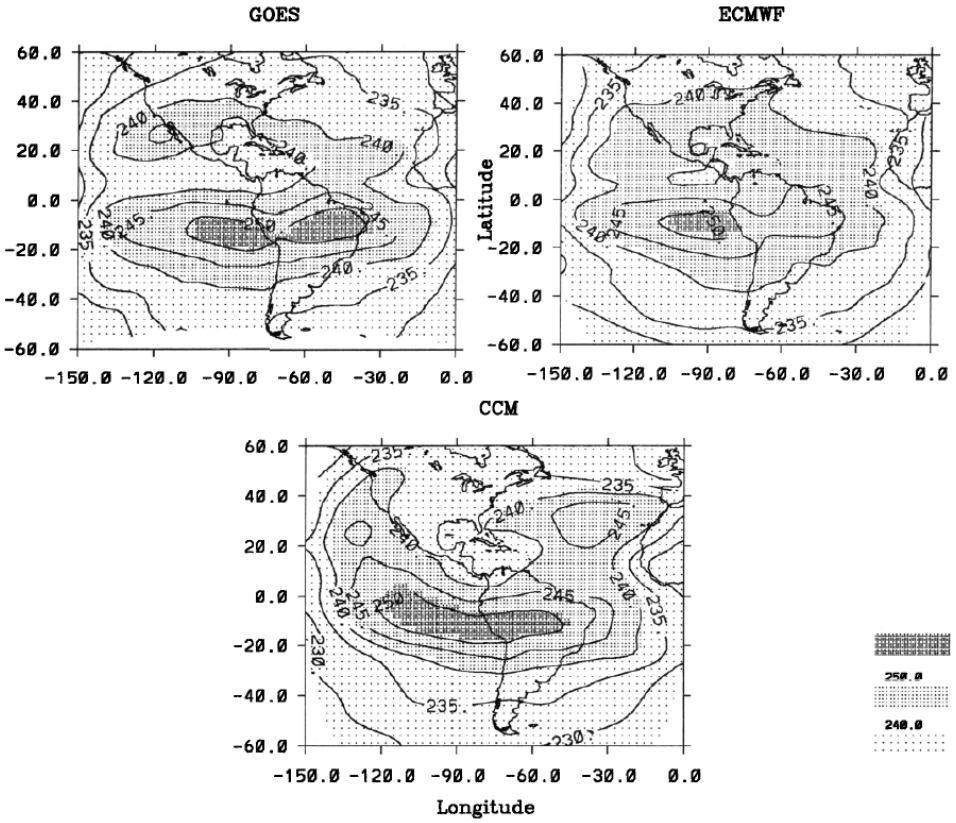


*Figure 5: Monthly mean $T_{6.7}$ (in K) from GOES observations, ECMWF analyses, and CCM simulations for July 1987 (from Soden and Bretherton, 1994).*

A different approach, although with the same aim of avoiding ambiguities in the comparisons between model variables and satellite retrievals, was followed by Klein and Jakob (1999) and Webb et al. (2001). They developed a piece of software called "the ISCCP simulator" that produces cloud retrievals from model fields that are directly comparable to the satellite retrievals. Since then, the ISCCP simulator has been successfully used by many modelling centres to evaluate the simulation of clouds (Zhang et al., 2005). The ISCCP retrieval classifies clouds according to their optical depth and cloud top pressure, as shown in Figure 6.

Webb et al. (2001) compared radiative fluxes and cloudiness fields (diagnosed with the ISCCP simulator) from three GCMs, using a combination of ERBE radiative fluxes and ISCCP cloud retrievals. Decomposing the cloud radiative effect into contributions from different layers (low, medium, and high) revelaed a tendency for the models' low-level clouds to compensate for errors in the shortwave radiative

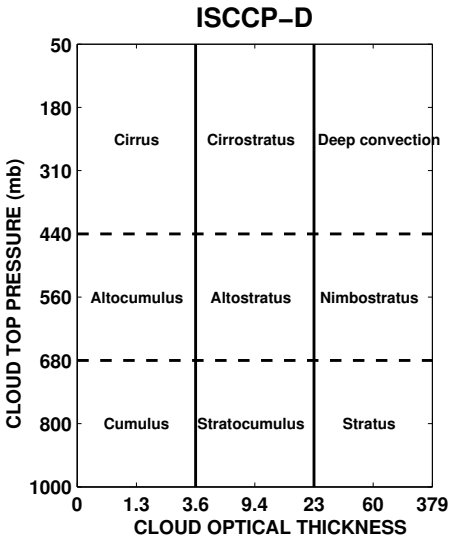


*Figure 6: Cloud-type definitions used in the ISCCP D-series dataset for daytime (from Rossow and Schiffer, 1999).*

fluxes caused by underestimates in mid- and high-level clouds.

## 4 Applications to the A-Train

The A-Train is a constellation of satellites that fly in formation in the same sunsyncronous orbit at 705 km of altitude and 98.2 degrees of inclination (Stephens et al., 2002). The composition of the A-Train prior to 2007 is depicted in Figure 7. In December 2007, there were slight changes to the positions of Aura and CloudSat within the formation (Stephens et al., 2008). This tightly controlled flight formation provides an unprecedented sinergy between instruments as they observe the same atmospheric column (except for the different sensor resolution) almost simultaneously. Among the suite of instruments available in the A-Train, the Cloud Profiling Radar (CPR) onboard CloudSat and the Cloud-Aerosol LIdar with Orthogonal Polarization (CALIOP) onboard CALIPSO (Cloud-Aerosol Lidar and Infrared Pathfinder Satellite Observations) are providing us with a new perspective on clouds and aerosols. CloudSat and CALIPSO were successfully launched on April 28, 2006. CloudSat CPR is the first millimeter wavelength radar in space, which operates at a frequency of 94 GHz (Im et al., 2005). The CPR points in the nadir direction, and its pulses sample a volume of 480 m in the vertical, with a horizontal resolution of 1.4 km across-track. The first CloudSat products (Stephens et al., 2008) were released on October 16th, 2006. Among these products is the CloudSat 2B-GEOPROF dataset, which provides the radar reflectivity, in dBZ, and identifies where hydrometeors occur (Mace et al., 2007). The primary instrument on board CALIPSO is the Cloud-Aerosol LIdar with Orthogonal Polarization (CALIOP), the first polarizitation lidar in space, operating at 532 nm and 1064 nm (Winker et al., 2007). CALIOP is nadir-pointing with a beam diameter of 70 meters at the Earth's surface, and a pulse repetition frequency that produces footprints every 333 m in the along-track direction. CALIPSO is able to detect thin cloud layers with optical depths of 0.01 or less, provided that the signal is averaged along-track (McGill et al., 2007). CALIPSO products are described by Vaughan et al. (2009). Among these products, the Vertical Feature Mask provides a target classification that gives information on the location and properties of aerosol and cloud layers.

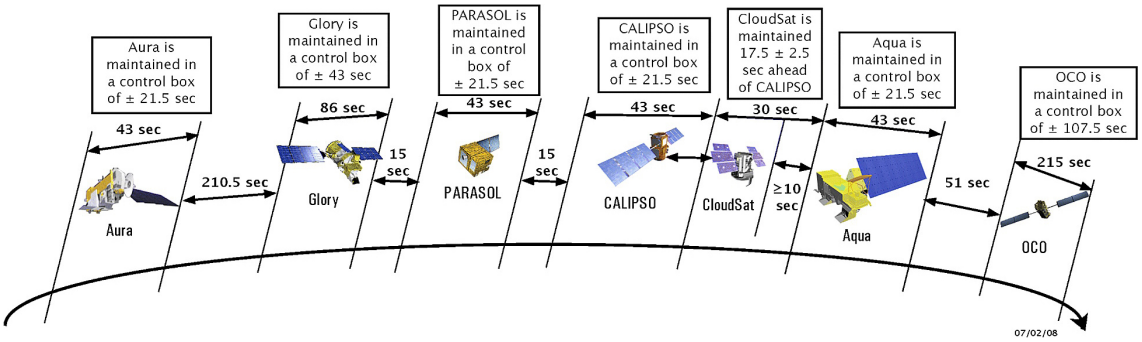


*Figure 7: The A-Train control boxes and the position of each member prior to December 2007 (from Stephens et al., 2008). The Orbiting Carbon Observatory (OCO) failed at launch on February 24, 2009.*

## 4.1 Model evaluation by using simulated CloudSat reflectivities

In order to make full use of CloudSat data for the evaluation of clouds, Bodas-Salcedo et al. (2008b) developed a system to simulate CloudSat data in the Met Office Unified Model (MetUM) that is consistent with the observations, taking into account the orbital path of the satellite. They applied this simulator to evaluate the MetUM global forecast model from two different points of view; on a case-study approach by analysing the direct comparisons of CloudSat passes over mid-latitude systems, and a more statistically-based approach by computing reflectivity histograms as function of height integrated over time. Figure 8 shows an example of the first approach. This figure clearly demonstrates the extra dimension that CloudSat gives by providing information on the vertical. The radar reflectivities as simulated from the model variables along that transect are shown in Figures 8a (sub-gridbox resolution) and 8b (gridbox resolution). The dotted contour lines show the atmospheric temperature as simulated by the model, with the 0$^o$C isotherm plotted with a solid line. As expected, a South-North gradient in temperature is observed with warmer temperatures in the South. On top of this background gradient, some discontinuities in the slope of the isotherms indicative of transitions between warm and cold sectors can also be identified. Overall, the model represents the vertical structure reasonably well, although there are noticeable differences from the observations (Figure 8c). From 0 to 500 km, the model simulates a cloud deck that is not seen by CloudSat. As CALIPSO is able to detect thinner clouds than CloudSat, Figure 8d helps to identify whether these cirrus clouds are spuriously generated by the model or present in reality. Although CALIPSO (Fig. 8d) sees high cloud in this first part of the transect, it is thinner than the cloud simulated by the model and higher, above 10 km. The sector from 500 to 1000 km is characterised by a multilayered cloud structure, with a high cloud layer between 9 and 12 km. Underneath this layer, is a second layer, between 5 and 7 km that is clearly visible by both CloudSat and CALIPSO. This mid-level cloud shows radar reflectivity factors between -20 and 0 dBZe, and attenuates the lidar signal most of the time. These two effects combined are an indication of mixed phase cloud (Hogan et al., 2003). Although the model produces cloud in this part of the system, it does not capture the multilayered structure seen in reality. The model also shows a strong signal in the radar reflectivity factor below the freezing level that is not seen in the CloudSat measurements. This signal comes from spurious drizzle generated by the model from boundary layer clouds. We cannot be certain whether or not these clouds are present in reality as the ability of CloudSat to detect non-precipitating boundary layer cloud is limited (Stephens et al., 2002), and the CALIPSO signal at these levels has been attenuated by the mixed phase cloud above. The sector from 1000 to 1400 km is characterised by the presence of hydrometeors from around 13 km (seen by CALIPSO) down to the ground. The CloudSat signal below 7 km seems to be dominated by precipitation, which sometimes causes strong attenuation at low levels. The freezing level can be clearly seen in the CloudSat signal in this part of the transect dominated by precipitation, with a significant increase in reflectivity with respect to the values just above the freezing

level (bright band). The origin and characteristics of the 94 GHz radar bright band (or its non-existence in non-precipitating clouds) is a topic of research currently under discussion in the literature (Sassen et al., 2005; Kollias and Albrecht, 2005; Sassen et al., 2007). The simulations show a more abrupt jump caused by the phase change from falling ice above the freezing level, to rainfall below it. This discontinuity is also caused by the different forward models used for these two hydrometeors.

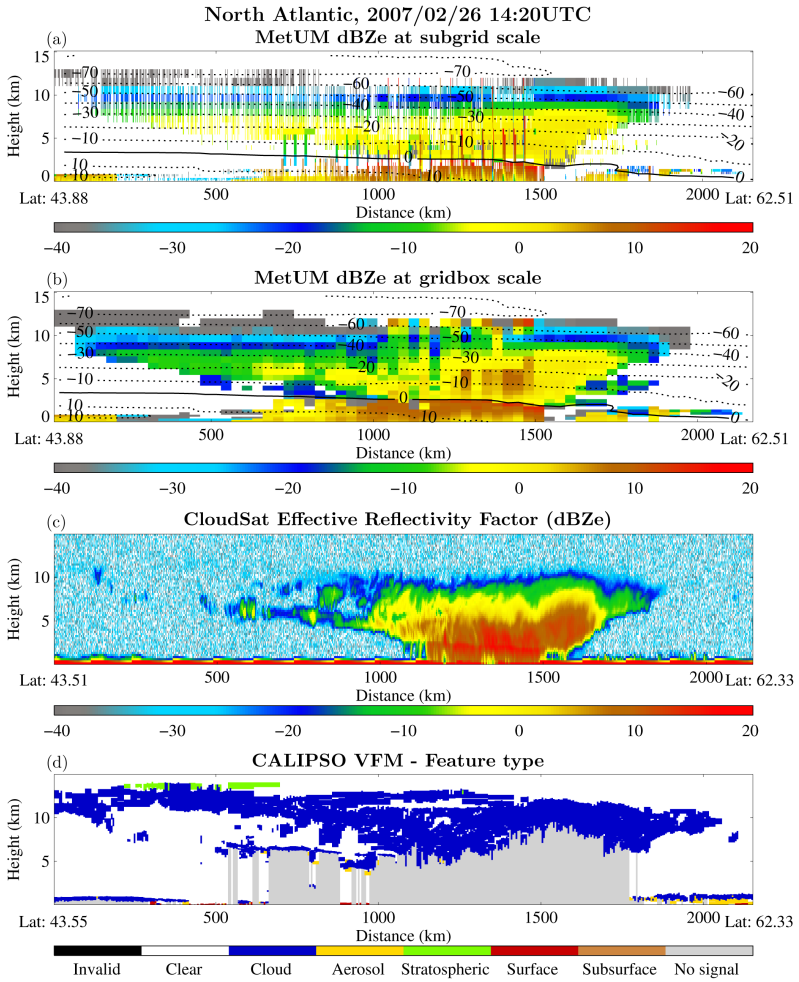


*Figure 8: Example of simulated mid-latitude system in the North Atlantic by the MetUM global forecast model on February 26$^{th}$, 2007: (a) simulated radar reflectivity (in dBZ) from the model outputs at sub-grid scale (b) simulated radar reflectivity (in dBZ) from the model outputs at sub-grid scale averaged over the model gridbox, (c) radar reflectivity observed by CloudSat, and (d) CALIPSO vertical feature mask. Contour lines in the model simulations show the simulated atmospheric temperature, with the 0$^o$C isotherm plotted with a solid line (from Bodas-Salcedo et al., 2008b).*

The simulated reflectivity values are significantly smaller than the observations for temperatures between -40$^o$C and -20$^o$C. The Cloudnet project provides systematic evaluation of cloud profiles in seven forecast models using ground observations (radar, lidar and microwave radiometer) (Illingworth et al., 2007). Cloudnet results for December 2006 over Chilbolton, UK, show that the MetUM global forecast model generally underestimates IWC by approximately a factor of 2 or more. Despite the fact that the mean uncertainty of current retrievals of IWC using radar is large ($\pm$66% as reported by Heymsfield et al. (2008) in an intercomparison study), the underestimation of simulated IWC seems to be the most likely explanation for the low bias in the reflectivities. This is also supported by recent comparisons of model IWC against aircraft measurements [*Baran et al., unpublished*].

Bodas-Salcedo et al. (2008b) also constructed reflectivity histograms as function of height in 2.5$^o$ by

2.5° regions for the 3-month period, from December 2006 to February 2007. They divided the vertical axis of these histograms in bins of 1 km, and the horizontal axis in bins of 2.5 dBZe. Figure 9 shows the model and observation histograms for a region covering the tropical warm pool (70°E - 150°E , 5°S - 20°N ). The observations sample a roughly triangular region in this 2D space. This region is limited on its left-hand side by the sensitivity limit of the CPR (approx. -30 dBZ). There seems to be a linear relationship between maximum reflectivity and height that we shall analyse in more detail below. Low levels, below 3 km, seem to show a slightly bimodal distribution, with a peak around -25 dBZ, and a second maximum near 5 dBZ. A very light drizzle flux of 0.001 mm $hr^{-1}$ can dominate the radar reflectivity at 94 GHz and produce a reflectivity of -20 dBZ (O'Connor et al., 2005). The LWC needed to produce a reflectivity of -20 dBZ is around 0.3 g $m^{-3}$, so -20 dBZ can be considered as an approximate threshold to define a drizzling cloud. The transition in the observations is smooth (non-drizzle - drizzle - rainfall), with highly populated bins in between. The lowest 1-km layer is not shown in the CloudSat plot due to the effect of the contamination by ground clutter.

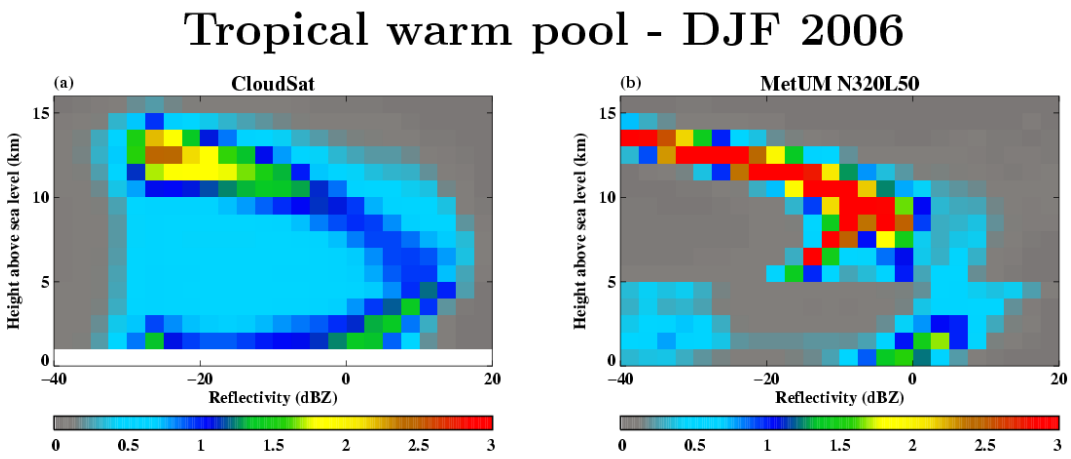


*Figure 9: Comparison of DJF 2006-2007 statistics for the tropical warm pool region: (a) joint height-reflectivity hydrometeor frequency of occurrence as observed by CloudSat, and (b) simulated by the MetUM global forecast model (%) (from Bodas-Salcedo et al., 2008b).*

In order to understand the different regions of this histogram and its relation with the microphysics, it is useful to remember that in the Rayleigh scattering regime, the reflectivity is the sixth moment of the particle size distribution (PSD) (e.g. Sauvageot, 1992). Given the PSD and the particle mass-size, the Rayleigh reflectivity can be expressed as a function of moments of the PSD that are related to model variables, like the hydrometeor water content and the number concentration (Bodas-Salcedo et al., 2008b). Then, a multiplicative correction to the Rayleigh reflectivity can be applied to account for Mie effects (Benedetti et al., 2003), and finally the attenuation by the atmospheric column between the radar and the target has to be taken into account. There are three clusters that are clearly visible in this histogram: the ice branch that goes from high altitude and low reflectivities (ice crystals) to the freezing level ($\approx 5km$ high) with high reflectivities (large aggregates). The precipitation cluster in the lower-right part of the plot (large liquid particles) and the non-precipitating liquid cloud in the lower-left part of the plot (small, liquid particles).

In the ice branch, the strength of the signal grows as height decreases due to aggregation that produces larger particles. Once the falling ice reaches the freezing level, located at ≈5 km in the tropical atmosphere, it melts and falls as rain. The radar signal at 94GHz is strongly attenuated by rainfall, which explains the change in slope between the ice and rainfall branches. The height-Ze relationship of the ice branch is also present in the simulations, although they show a lack of smaller reflectivities at those levels (Fig. 9b). This region of the histogram that is not sampled by the model is the region that Zhang

et al. (2007) labelled as cumulus congestus in their clustering analysis of CloudSat data. The model explores a much smaller range of reflectivities, with the majority of points clustered around a much tighter height-reflectivity relationship. At lower levels, the model seems to operate in two regimes, one with non-precipitating cloud (reflectivities ≈ -30 dBZ), and the other for precipitating cloud (reflectivities ≈ 0 dBZ).

### 4.2 Model evaluation by using simulated lidar backscatter

(Chepfer et al., 2008) followed a similar approach that the one presented above for CloudSat but for the simulation of the CALIPSO lidar backscatter signal. They used CALIPSO lidar observations toghether with a lidar simulator to evaluate the cloudiness simulated by a climate model. They clearly show how the forward modelling approach make comparisons with observations fairer by showing the differences between the three dimensional distribution of cloud fraction as simulated by the model and that computed from the simulated lidar backscatter (Fig. 10).

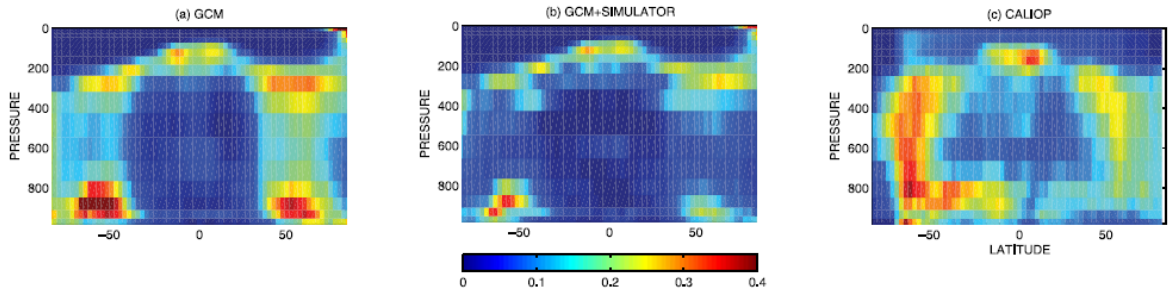


*Figure 10: Zonally-averaged cloud fraction for January-February-March: (a) original cloud fraction predicted by the GCM, (b) GCM cloud fraction diagnosed from the lidar simulator, and (c) cloud fraction derived from CALIOP/CALIPSO data (from Chepfer et al., 2008).*

## 5 An integrated approach: COSP

In order to take advantage of this new picture of the atmosphere provided by the A-Train, the Cloud Feedback Model Intercomparison Project (CFMIP) community decided to develop an integrated satellite simulator, the CFMIP Observational Simulator Package (COSP) (Bodas-Salcedo et al., in preparation). COSP is a flexible software tool that enables the simulation of data from several satellite-borne sensors from model variables. Especially, COSP will take advantage of the synergy provided by the active sensors on the A-Train, CloudSat and CALIPSO. It facilitates the use of satellite data to evaluate models in a process-oriented and consistent way. The flexibility of COSP makes it suitable to be used in any type of numerical model, from high-resolution cloud-resolving models to coarse-resolution models like the GCMs used in the IPCC, and the scales in between used in weather forecast models. The fact that COSP includes several simulators under the same interface facilitates the implementation of a range of simulators in models.

The current version of COSP includes simulators for the following instruments: CloudSat radar (Haynes et al., 2007), CALIPSO lidar (Chepfer et al., 2008), ISCCP (Klein and Jakob, 1999; Webb et al., 2001), and the Multiangle Imaging SpectroRadiometer (MISR) (Marchand et al., in preparation). New releases of COSP will include two extra simulators: one for the Moderate Resolution Imaging Spectroradiometer (MODIS) and the fast radiative transfer code RTTOV (Saunders et al., 1999). There is also work ongoing to develop and include a simulator for the Tropical Rainfall Measuring Mission (TRMM), both

| CloudSat |
|---|
| Radar reflectivity |
| Height-reflectivity histograms |
| **CALIPSO** |
| Lidar total backscatter (532 nm) |
| Lidar molecular backscatter |
| Height-scattering ratio histograms |
| Low-level cloud fraction (CTP $>$ 680 hPa) |
| Mid-levlel cloud fraction (440 $<$ CTP $<$ 680 hPa) |
| High-level cloud fraction (CTP $<$ 440 hPa) |
| 3D Cloud fraction |
| Total cloud fraction |
| PARASOL mono-directional reflectance |
| **MISR** |
| MISR CTH-Tau histograms |

| ISCCP |
|---|
| Mean cloud albedo |
| Cloud optical depth in each subcoumn |
| Mean cloud top pressure |
| Mean 10.5 micron brightness temperature |
| Mean clear-sky 10.5 micron brightness temperature |
| Mean cloud optical depth |
| Cloud top pressure in each subcolumn |
| CTP-tau histograms |
| Total cloud fraction |
| **Combined diagnostics** |
| Total cloud fraction from CALIPSO and CloudSat |
| 3D cloud fraction as seen from CALIPSO but not CloudSat |

*Table 2: List of diagnostics from the COSP v1.1.*

for the precipitation radar and for the passive microwave radiometers. Table 2 lists the output diagnostics from the current version of COSP (v1.1). The Climate Model Output Rewriter (CMOR) library is used to write the ouputs to NetCDF files that comply with the Climate and Forecast (CF) Metadata Convention and fulfill the requirements of the climate community's standard model experiments. The Working Group on Coupled Modelling (WGCM) has recommended the use of COSP for the 5th Intergovernmental Panel on Climate Change (IPCC) assessment report (AR), the Coupled Model Intercomparison Project Phase 5 (CMIP5). CMIP is a standard experimental protocol for studying the output of coupled ocean-atmosphere general circulation models (GCMs). It provides a community-based infrastructure in support of climate model diagnosis, validation, intercomparison, documentation and data access (Meehl et al., 2007). Some COSP outputs will be included into the set of CMIP5 outputs (`http://cmip-pcmdi.llnl.gov/cmip5/experiment_design.html`). COSP is open source software and can be downloaded from the CFMIP website without charge (`www.cfmip.net`).

A sample of output output diagnostics is shown in Figure 11. It shows the global average of four diagnostics from one timestep of the atmosphere-only version of the Hadley Centre Global Environmental Model version 1, HadGEM1 (Johns et al., 2006).

## 6 Conclusions

A brief review on the application of satellite data in model model evaluation has been presented. It has been argued that satellite retrievals introduce structural uncertainties that make their use difficult for quantitative evaluation of NWP and climate models, and that forward modelling avoids some of these uncertainties because it brings models and observations onto the same ground. It also provides an easy framework where sensitivity tests can be carried out. The main caveat of this approach is that the interpretation has to be done in the observations space, which perhaps makes more difficult to extract conclusions in terms of geophysical variables.

Applications of forward modelling to the active instruments on the A-train have been described, and in particular recent work on the use of simulated CloudSat reflectivities for model evaluation has been presented. This study is a demonstration of a possible way to use CloudSat data to evaluate numerical models. There are also other topics that deserve attention. CloudSat can provide information about microphysical processes on a global basis (e.g. Stephens and Haynes, 2007) and their relation to the dynamics through their impact in the radiative heating profiles. This new global capabilities need to be explored in the future.

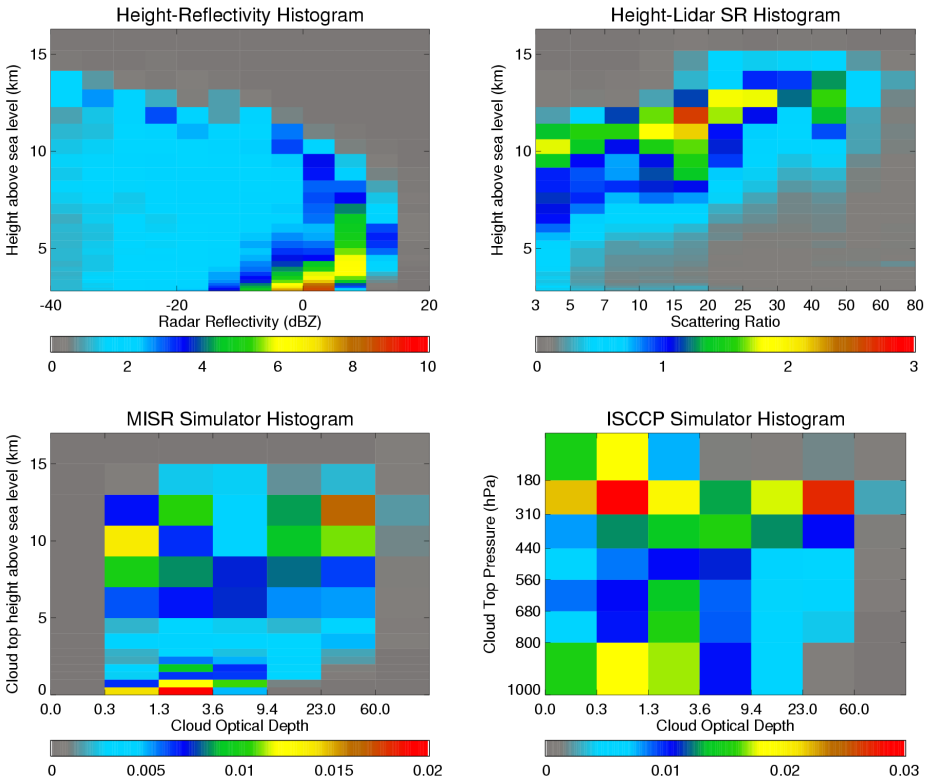


*Figure 11: Examples of COSP diagnostics: (a) frequency of occurrence of radar reflectivity as function of height, (b) frequency of occurrence of lidar scattering ratio as function of height, (c) CTP-tau histogram from the ISCCP siulator, and (d) CTH-tau histogram from the MISR simulator.*

The CFMIP Observational Simulator Package (COSP) has been developed in recent years. COSP is a multi-instrument satellite simulator package that aims to exploit the new observing capabilities that provide the A-Train (and satellites in general) for model evaluation and understanding of cloud and radiation processes. A brief description of COSP has been presented with examples of its capabilities.

## Acknowledgements

The author is supported by the Joint DECC and Defra Integrated Climate Programme - DECC/Defra (GA01101). The author would like to thank the ECMWF for the invitation to present at this annual seminar. Especial thanks to M. J. Webb, M. A. Ringer, Y. Tsushima and J. Williams for their comments and contributions to this paper. COSP has been developed by a collaboration between several institutions: Met Office, Laboratoire de Météorologie Dynamique/Institut Pierre-Simon Laplace, Lawrence Livermore National Laboratory, University of Washington, and Colorado State University.

## References

Allan, R. P., A. Slingo, S. F. Milton, and M. E. Brooks, 2007: Evaluation of the Met Office global forecast model using Geostationary Earth Radiation Budget (GERB) data. *Q. J. R. Meteorol. Soc.*, **133**, 1993–2010, doi:10.1002/qj.166.

Benedetti, A., G. L. Stephens, and J. M. Haynes, 2003: Ice cloud microphysics retrievals from millimeter

radar and visible optical depth using an estimation theory approach. *J. Geophys. Res.*, **108**, 4335, doi: 10.1029/2002JD002693.

Bodas-Salcedo, A., M. A. Ringer, and A. Jones, 2008a: Evaluation of the surface radiation budget in the atmospheric component of the Hadley Centre Global Environmental Model (HadGEM1). *J. Climate*, **21**, 4723–4748, doi:10.1175/2008JCLI2097.1.

Bodas-Salcedo, A., M. J. Webb, M. E. Brooks, M. A. Ringer, K. D. Williams, S. F. Milton, and D. R. Wilson, 2008b: Evaluating cloud systems in the met office global forecast model using simulated cloudsat radar reflectivities. *J. Geophys. Res.*, **113**, D00A13, doi:10.1029/2007JD009620.

Bodas-Salcedo, A., et al., in preparation: COSP: a multi-instrument satellite simulator for model evaluation. *Bull. Am. Meteorol. Soc.*

Chepfer, H., S. Bony, D. Winker, M. Chiriaco, J.-L. Dufresne, and G. Sèze, 2008: Use of CALIPSO lidar observations to evaluate the cloudiness simulated by a climate model. *Geophys. Res. Lett.*, **35**, L15 704, doi:10.1029/2008GL034207.

Eyre, J. R., 1987: On systematic errors in satellite sounding products and their climatological mean values. *Q. J. R. Meteorol. Soc.*, **113**, 279–292, doi:10.1002/qj.49711347516.

Gates, W. L. and 15 coauthors, 1999: An overview of the results of the Atmospheric Model Intercomparison Project (AMIP I). *Bull. Am. Meteorol. Soc.*, **80 (1)**, 29–55.

Gates, W. L., et al., 1999: An overview of the results of the Atmospheric Model Intercomparison Project (AMIP I). *Bull. Am. Meteorol. Soc.*, **80 (1)**, 29–55.

Haynes, J. M., R. T. Marchand, Z. Luo, A. Bodas-Salcedo, and G. L. Stephens, 2007: A multipurpose radar simulation package: Quickbeam. *Bull. Am. Meteorol. Soc.*, **88 (11)**, 1723–1727, doi: 10.1175/BAMS-88-11-1723.

Heymsfield, A. J., et al., 2008: Testing IWC retrieval methods using radar and ancillary measurements with in situ data. *J. Appl. Meteorol. Clim.*, **47**, 135–163, doi:10.1175/2007JAMC1606.1.

Hogan, R. J., P. N. Francis, H. Flentje, A. J. Illingworth, M. Quante, and J. Pelon, 2003: Characteristics of mixed-phase clouds. i: Lidar, radar and aircraft observations from CLARE'98. *Q. J. R. Meteorol. Soc.*, **129**, 2089–2116, doi:10.1256/qj.01.208.

Illingworth, A. J., et al., 2007: CLOUDNET: continuous evaluation of cloud profiles in seven operational models using ground-based observations. *Bull. Am. Meteorol. Soc.*, **88**, 883–898, doi:10.1175/BAMS-88-6-883.

Im, E., C. Wu, and S. L. Durden, 2005: Cloud profiling radar for the CloudSat mission. *IEEE Aero. El. Sys. Mag.*, **20 (10)**, 15–18, doi:10.1109/MAES.2005.1581095.

Johns, T. C., et al., 2006: The new Hadley Centre climate model HadGEM1: Evaluation of coupled simulations. *J. Climate*, **19 (7)**, 1327–1353.

Klein, S. A. and C. Jakob, 1999: Validation and sensitivities of frontal clouds simulated by the ECMWF model. *Mon. Weather Rev.*, **127 (10)**, 2514–2531.

Kollias, P. and B. Albrecht, 2005: Why the melting layer radar reflectivity is not bright at 94 GHz. *Geophys. Res. Lett.*, **32**, L24 818, doi:10.1029/2005GL024074.

Liou, K. N., 2002: *An introduction to atmospheric radiation*. 2d ed., International Geophysics Series, Academic Press.

Mace, G. G., R. Marchand, Q. Zhang, and G. Stephens, 2007: Global hydrometeor occurrence as observed by CloudSat: Initial observations from summer 2006. *Geophys. Res. Lett.*, **34**, L09 808, doi: 10.1029/2006GL029017.

Marchand, R., T. Ackerman, M. Smyth, and B. Rossow, in preparation: A comparison of cloud top height and optical depth histograms from MISR, ISCCP and MODIS. *J. Geophys. Res.*

McGill, M. J., M. A. Vaughan, C. R. Trepte, W. D. Hart, D. L. Hlavka, D. M. Winker, and R. Kuehn, 2007: Airborne validation of spatial properties measured by the CALIPSO lidar. *J. Geophys. Res.*, **112 (D20)**, D20 201, doi:10.1029/2007JD008768.

Meehl, G. A., et al., 2007: Global climate projections. *Climate Change 2007: The Physical Science Basis. Contribution of Working Group I to the Fourth Assessment Report of the Intergovernmental Panel on Climate Change*, S. Solomon, D. Qin, M. Manning, Z. Chen, M. Marquis, K. B. Averyt, M. Tignor, and H. L. Miller, Eds., Cambridge University Press.

Morcrette, J. J., 1991: Evaluation of model-generated cloudiness: Satellite-observed and model-generated diurnal variability of brightness temperature. *Mon. Weather Rev.*, **119 (5)**, 1205–1224, doi:10.1175/1520-0493(1991)119¡1205:EOMGCS¿2.0.CO;2.

O'Connor, E. J., R. J. Hogan, and A. J. Illingworth, 2005: Retrieving stratocumulus drizzle parameters using doppler radar and lidar. *J. Appl. Meteorol.*, **44**, 14–27.

Ringer, M. A., J. M. Edwards, and A. Slingo, 2003: Simulation of satellite channel radiances in the Met Office Unified Model. *Q. J. R. Meteorol. Soc.*, **129**, 1169–1190, doi:10.1256/qj.02.61.

Rossow, W. B. and R. A. Schiffer, 1999: Advances in understanding clouds from ISCCP. *Bull. Am. Meteorol. Soc.*, **80**, 2261–2287.

Salathé, E. P. and D. Chesters, 1995: Variability of moisture in the upper troposphere as inferred from tovs satellite observations and the ecmwf model analyses in 1989. *J. Climate*, **8**, 120–132, doi: 10.1175/1520-0442(1995)008¡0120:VOMITU¿2.0.CO;2.

Sassen, K., J. R. Campbell, J. Zhu, P. Kollias, M. Shupe, and C. Williams, 2005: Lidar and triple-wavelength doppler radar measurements of the melting layer: A revised model for dark- and bright-band phenomena. *J. Appl. Meteorol.*, **44**, 301–312.

Sassen, K., S. Matrosov, and J. Campbell, 2007: CloudSat spaceborne 94 GHz radar bright bands in the melting layer: An attenuation-driven upside-down lidar analog. *Geophys. Res. Lett.*, **34**, L16 818, doi:10.1029/2007GL030291.

Saunders, R., M. Matricardi, and P. Brunel, 1999: An improved fast radiative transfer model for assimilation of satellite radiance observations. *Q. J. R. Meteorol. Soc.*, **125**, 1407–1425.

Sauvageot, H., 1992: *Radar Meteorology*. Artech House.

Slingo, J. M., 1982: A study of the earth's radiation budget using a general circulation model. *Q. J. R. Meteorol. Soc.*, **108**, 379–405, doi:10.1002/qj.49710845606.

Smith, R. N. B., 1990: A scheme for predicting layer clouds and their water content in a general circulation model. *Q. J. R. Meteorol. Soc.*, **116**, 435–460.

Soden, B. J. and F. P. Bretherton, 1994: Evaluation of water vapor distribution in general circulation models using satellite observations. *J. Geophys. Res.*, **99 (D1)**, 1187–1210.

Stephens, G. L. and J. M. Haynes, 2007: Near global observations of the warm rain coalescence process. *Geophys. Res. Lett.*, **34**, L20 805, doi:10.1029/2007GL030259.

Stephens, G. L. and C. D. Kummerow, 2007: The remote sensing of clouds and precipitation from space: A review. *J. Atmos. Sci.*, **64 (11)**, 3742–3765, doi:10.1175/2006JAS2375.1.

Stephens, G. L., et al., 2002: The CloudSat mission and the A-Train. *Bull. Am. Meteorol. Soc.*, **83**, 1771–1790.

Stephens, G. L., et al., 2008: Cloudsat mission: Performance and early science after the first year of operation cloudsat mission: Performance and early science after the first year of operation. *J. Geophys. Res.*, **113**, D00A18, doi:10.1029/2008JD009982.

Thomas, G. E. and K. Stamnes, 2002: *Radiative transfer in the atmosphere and ocean*. 2d ed., Cambridge Atmospheric and Space Science Series, Cambridge University Press.

Vaughan, M. A., et al., 2009: Fully automated detection of cloud and aerosol layers in the CALIPSO lidar measurements. *J. Atmos. Oceanic Technol.*, **26 (10)**, 2034–2050, doi: 10.1175/2009JTECHA1228.1.

Webb, M., C. Senior, S. Bony, and J. J. Morcrette, 2001: Combining ERBE and ISCCP data to assess clouds in the Hadley Centre, ECMWF and LMD atmospheric climate models. *Clim. Dyn.*, **17**, 905–922.

Winker, D. M., W. H. Hunt, and M. J. McGill, 2007: Initial performance assessment of CALIOP. *Geophys. Res. Lett.*, **34**, L19 803, doi:10.1029/2007GL030135.

Zhang, M. H., et al., 2005: Comparing clouds and their seasonal variations in 10 atmospheric general circulation models with satellite measurements. *J. Geophys. Res.*, **110 (D15)**.

Zhang, Y., S. Klein, G. G. Mace, and J. Boyle, 2007: Cluster analysis of tropical clouds using cloudsat data. *Geophys. Res. Lett.*, **34**, L12 813, doi:10.1029/2007GL029336.